IEEE Photonics Journal
An IEEE Photonics Society Publication

Open Access

A Four-Channel DWDM Tunable Add/Drop Demultiplexer Based on Silicon Waveguide Bragg Gratings

Volume 11, Number 1, February 2019

Debin Mu
Huiye Qiu
Jianfei Jiang
Xiaofei Wang
Zhilei Fu
Yuehai Wang
Xiaoqing Jiang
Hui Yu
Jianyi Yang

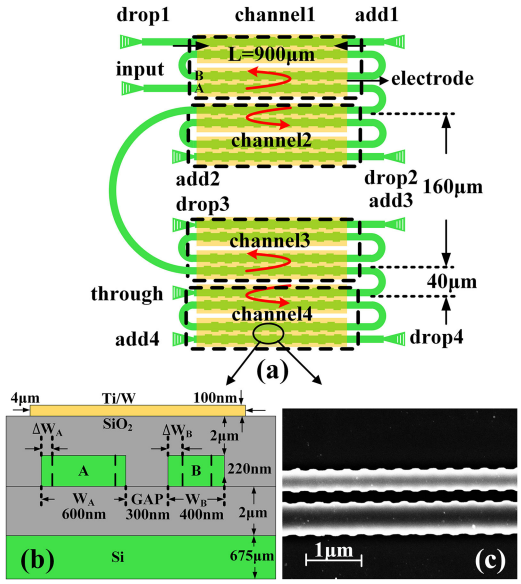

DOI: 10.1109/JPHOT.2019.2897359

IEEE photonics SOCIETY

IEEE

A Four-Channel DWDM Tunable Add/Drop Demultiplexer Based on Silicon Waveguide Bragg Gratings

Debin Mu,[1] Huiye Qiu,[2] Jianfei Jiang,[1] Xiaofei Wang,[1] Zhilei Fu,[1] Yuehai Wang,[1] Xiaoqing Jiang,[1] Hui Yu,[1] and Jianyi Yang[1]

[1]Institute of Microelectronics and Nanoelectronics, College of Information Science and Electronics Engineering, Zhejiang University, Hangzhou 310027, China
[2]Department of Mechanical and Electrical Engineering, Longyan University, Longyan 364012, China

DOI:10.1109/JPHOT.2019.2897359

Manuscript received December 25, 2018; revised January 27, 2019; accepted January 30, 2019. Date of publication February 4, 2019; date of current version February 18, 2019. This work was supported in part by the National Key R&D Program of China under Grant 2016YFB0402505, in part by Zhejiang Provincial Natural Science Foundation for Distinguished Young Scholar (LR15F050002), and in part by Fujian Province Science Foundation of China (JZ160479). Corresponding author: Hui Yu (e-mail: huiyu@zju.edu.cn).

Abstract: We demonstrate a thermally tunable four-channel add/drop demultiplexer based on silicon grating-assisted contra-directional couplers (contra-DCs) for 200 GHz dense wavelength division multiplexing (DWDM) systems. In order to obtain the narrow bandwidth and the rapid roll-off necessary for the DWDM, every wavelength channel is filtered dually by two identical contra-DCs cascaded in parallel. In addition, the phase apodization technique is utilized to suppress sidelobes. With these special designs, passbands of the four drop ports exhibit 3 and 20 dB bandwidths of 0.4 and 0.8 nm, respectively, while isolation between adjacent channels is better than 20 dB. Insertion losses at through and drop ports are 0.6 and ∼2.6 dB, respectively. The maximal wavelength-tunable range is up to 25 nm.

Index Terms: Integrated optics device, gratings, demultiplexer, waveguides, DWDM, filter.

1. Introduction

Wavelength division multiplexing (WDM) is undoubtedly the leading technology to drastically increase transmission capacities of silicon photonic integrated circuits [1], [2]. If one needs to manipulate only one or a few wavelength channels in a dense WDM system rather than demultiplex all channels simultaneously, ring resonators are usually preferred among various wavelength filters thanks to the merits of compact footprint, easy cascadability and tunability, sharp filtering curve, etc [3], [4]. Despite these advantages, a ring resonator is usually subjected to a limited free spectral range (FSR) and strong nonlinear effects induced by the resonance enhancement inside the cavity [5]. The FSR sets a cap on the maximum channel count of a WDM system. Although the FSR can be extended significantly by cascading multi rings with different radii, this approach complicates both design and active control of rings [6]. On the other hand, nonlinear effects constrain the high power handing ability of the ring resonator, which is highly desired by many microwave photonics systems [7].

Besides ring resonators, the functionality of add/drop filtering could also be implemented by waveguide Bragg gratings (WBG). One typical configuration is the grating assisted contra-directional coupler (DC) which enables a wavelength-selective back-coupling between fundamental modes of two neighboring waveguides [8], [9]. Another prevailing configuration is the multimode waveguide with asymmetric sidewall grating which enables a wavelength-selective back-coupling between TE_0 and TE_1 modes of the same waveguide [10], [11]. The distributed feedback nature of WBGs makes these filters be free of the FSR limitation, and less susceptible to nonlinear effects that could distort filtering characteristics at high optical power levels. Thanks to these advantages, silicon WBG filters have been successfully utilized to build four-channel coarse WDM systems with a channel spacing of 6 nm in [12], and with a 1 dB bandwidth of 370 GHz in [13]. However, very few multi-channel dense WDM (DWDM) systems have been demonstrated with silicon WBG filters. The challenge originates from two factors: Firstly, the large refractive index contrast of Si/SiO_2 waveguide system implies that grating teeth induce a strong dielectric perturbation, which in turn leads to a large coupling coefficient between the two interacting modes. According to the coupled mode theory, the 3 dB bandwidth of a Bragg grating increases with the coupling coefficient. In principle, a narrow 3 dB bandwidth can be obtained by reducing the corrugation width of the grating. However, the demanded very shallow corrugation of less than 20 nm is very difficult to realize with the state-of-the-art micro fabrication process. Secondly, an inherent drawback of the Bragg grating is the existence of sidelobes, which lead to a high crosstalk between two closely-spaced wavelength channels of a DWDM system. To address this issue, ring resonators and WBG filters are combined in [14] to form a 1 by 4 FSR free multiplexer, whose 3 dB bandwidth is as narrow as 0.5 nm.

In this paper, a thermally tunable four-channel DWDM demultiplexer based on silicon grating assisted contra-DCs is demonstrated. Following measures are utilized so as to obtain a sharp channel selection ability together with a high sidelobe suppression ratio (SLSR): Firstly, by tailoring dimensions of the two adjacent waveguides and the widths of their sidewall corrugations, we adjust the coupling coefficient of the contra-DC to obtain a narrow bandwidth. Secondly, a pair of identical grating assisted contra-DCs are cascaded to add/drop a single wavelength channel [15]. A repeated filtering at the same central wavelength enables a rapid roll-off of the spectrum and thus reduces the 3 dB bandwidth furthermore. Thirdly, the phase apodization technique we proposed in [16] is utilized to suppress sidelobes on both sides of the central wavelength. With these special measures, the pass band of the filter exhibits 3 dB and 20 dB bandwidths of 0.4 nm and 0.8 nm, respectively, while the SLSR is 26 dB. The isolation between two adjacent channels with a 1.6 nm wide spacing is larger than 20 dB. To the best of our knowledge, this is the first report of multi-channel DWDM demultiplexer based on silicon WBG filters.

2. Operation Principle and Design

A schematic diagram of the four-channel demultiplexer is shown in Fig. 1. The device consists of four pairs of identical grating assisted contra-DCs which are connected in series by a bus waveguide. It is well known that under the phase matching condition, a grating assisted contra-DC reflects the input mode from one waveguide to the other waveguide as indicated by the red arrows in Fig. 1(a) [17]. In order to reduce the bandwidth, we connect two identical contra-DCs in the manner shown in Fig. 1(a). Specifically, the drop and the add ports of the first contra-DC are connected to the input and the through ports of the second contra-DC, respectively. If signals at the central wavelength of the grating are incident on the input and the add ports, they will be routed to the drop port and the bus waveguide, respectively, after being reflected twice. Compared with one single grating assisted contra-DC, the grating assisted contra-DC pair provides much steeper passband edges. Although the two WBGs of each channel form a loop in Fig. 1(a), the ring resonance effect inside this loop is actually negligible as long as back coupling coefficients at the two contra-directional coupling regions are strong. All eight grating assisted contra-DCs have independent metallic heaters on top as shown in Fig. 1(b). Each electrode heats up both waveguides of a grating assisted contra-DC together so as to adjust its central wavelength [18], [19]. Fiber grating couplers are used to interface the device with input and output single mode fibers [20].

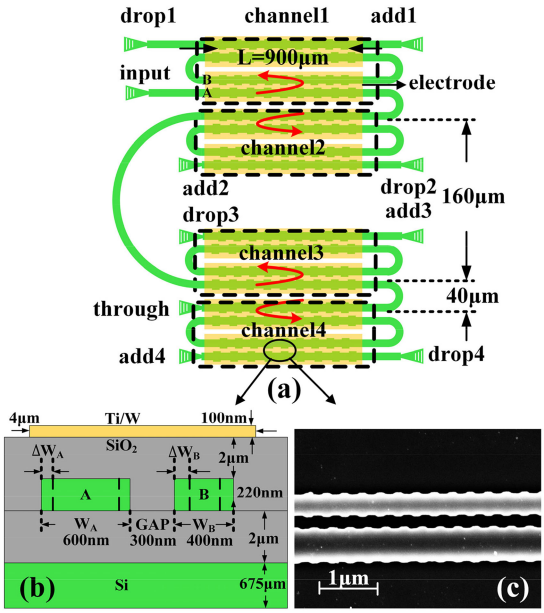

Fig. 1. (a) Schematic diagram of the four-channel DWDM demultiplexer. (b) Cross-section of the silicon grating-assisted contra-DC with the heater. (c) Top view SEM image of the fabricated grating-assisted contra-DC.

The grating assisted contra-DCs are designed with special attention to reduce their bandwidths. As shown in Fig. 1(b), the widths of the two coupled strip waveguides are 400 nm and 600 nm, respectively, to avoid excitation of high-order modes. The 200 nm difference in waveguide width is beneficial to eliminate the co-directional coupling between the two waveguides. The gap between two waveguides is 300 nm. Sidewall corrugations etched along the two strip waveguides have a pitch of $\Lambda = 318$ nm which meets the phase matching condition. The total length of the sidewall grating is L $= 900$ μm. Theoretically, increasing the grating length helps to enhance the back coupling coefficient of a grating assisted contra-DC and thus reduce the insertion loss of the drop port. However, performances of long waveguide gratings are very susceptible to fabrication imperfections such as variances of waveguide dimensions along the grating, uneven thicknesses of Si and SiO_2 layers, and so on. Resultant spectral responses are distorted and hence present reduced extinction ratios and strong ripples. Taking these factors into account, we set a grating length of 900 μm according to the quality of the microfabrication process used. The bending radius of the waveguide is 20 μm and 80 μm as shown in Fig. 1(a). The distance between two adjacent electrodes is set further than 20 μm to avoid thermal crosstalk. The electrode width is 4 μm, which is wide enough to cover the two coupled waveguides.

We utilize the phase apodization technique to suppress sidelobes. Conventional apodization methods which modulate recessing amplitude or duty cycle of the corrugation could only suppress sidelobes on the long-wavelength side of the center wavelength [21]. To address this issue, we have developed a phase apodization technique which is able to suppress sidelobes on both sides of the center wavelength in [16]. As shown in Fig. 2(a), this technique utilizes a uniform grating of 50% duty cycle for waveguide A, while each tooth of waveguide B is offset by ΔL with respect to the tooth of waveguide A that locates in the same longitudinal period.

The value of ΔL is modulated along the z direction by a Gaussian function, and can be written as

$$\Delta L = \frac{\Lambda}{2}\left(1 - e^{-a\frac{(z-0.5L)^2}{L^2}}\right) \tag{1}$$

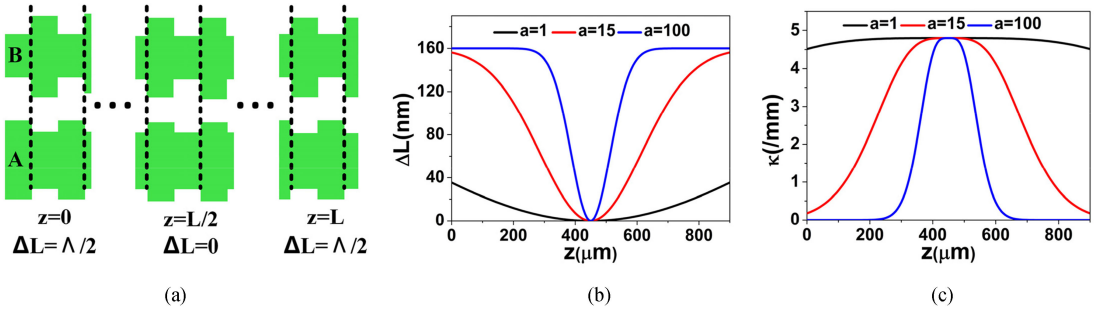

Fig. 2. (a) Schematic diagram of the phase apodization technique. (b) Calculated lateral misalignments of the apodized grating-assisted contra-DC. (c) coupling coefficients of the apodized grating-assisted contra-DC. The values of apodization coefficients are a = 1, 15, and 100 in the calculation.

where *a* is the apodization coefficient which influences the coupling coefficient. With this arrangement, the coupling coefficient κ of a grating assisted contra-DC can be calculated as [20]

$$\kappa = |\kappa_A + \kappa_B \exp(i * 2\pi\Delta L/\Lambda)| \tag{2}$$

where $2\pi\Delta L/\Lambda$ denotes the local phase difference between dielectric perturbations of the two waveguide gratings. κ_A and κ_B are the coupling coefficients calculated by replacing the grating B and the grating A with a straight waveguide, respectively, which can be written as

$$\kappa_{A/B} = \frac{\omega\varepsilon_0}{4}\iint E_A(x,y)\cdot\Delta n^2_{A/B}E^*_B(x,y)dxdy \tag{3}$$

where $E_{A/B}$ and $\Delta n_{A/B}$ denote electric filed distributions and refractive index perturbations in the two waveguides, respectively. If κ_A and κ_B are properly designed to be equal, i.e., $\kappa_A = \kappa_B = \kappa_0$, the coupling coefficient κ then can be written as

$$\kappa = 2\kappa_0\left|\cos(\pi\Delta L/\Lambda)\right| \tag{4}$$

At the middle of the device, the dielectric perturbations in the two waveguides are in phase, i.e., $\Delta L = 0$, so the coupling coefficient κ reaches the maximum, while its value reaches the minimum at the two ends of the grating. Therefore, the coupling coefficient can be apodized by tuning the local misalignment between teeth of the two gratings.

The coupling coefficient is determined by the overlap between the two guided modes and sidewall gratings. Since waveguide B is 200 nm wider than waveguide A, the TE_0 mode in waveguide B is less susceptible to the sidewall corrugation. In order to fulfill the condition $\kappa_A = \kappa_B$, corrugation in waveguide B should be wider than that in waveguide A. According to the coupled mode theory, a narrow bandwidth can be achieved by reducing the corrugation width. However, the minimal width is constrained by the practical fabrication resolution. Taking all these factors into account, the corrugation widths we choose for the narrow and the wide waveguides are $\Delta W_A = 25$ nm and $\Delta W_B = 40$ nm, respectively. Based on these parameters, we calculate variations of ΔL and κ along the longitudinal position with the apodization coefficient *a* as a variable. The results are plotted in Figs. 2(b) and 2(c). If the value of *a* is small, e.g., $a = 1$, the apodization effect of κ is very weak as shown in Fig. 2(c). On the other hand, if a large value is chosen for *a*, e.g., $a = 100$, the apodization occurs mainly in the central part of the grating. Neither case can effectively suppress sidelobes. In order to match the attenuation length of the coupling coefficient κ to *L*/2, we set an apodization coefficient of $a = 15$. The resultant apodization profile is displayed in Fig. 2(c).

3. Fabrication and Measurement Results

The devices are fabricated on a silicon-on-insulator (SOI) substrate with a 3-μm-thick SiO_2 layer and a 220-nm-thick Si layer. At first, Si waveguides are defined by the electron-beam lithography and the inductively coupled plasma dry-etching (ICP). After that, a 2-μm-thick SiO_2 layer is deposited by the

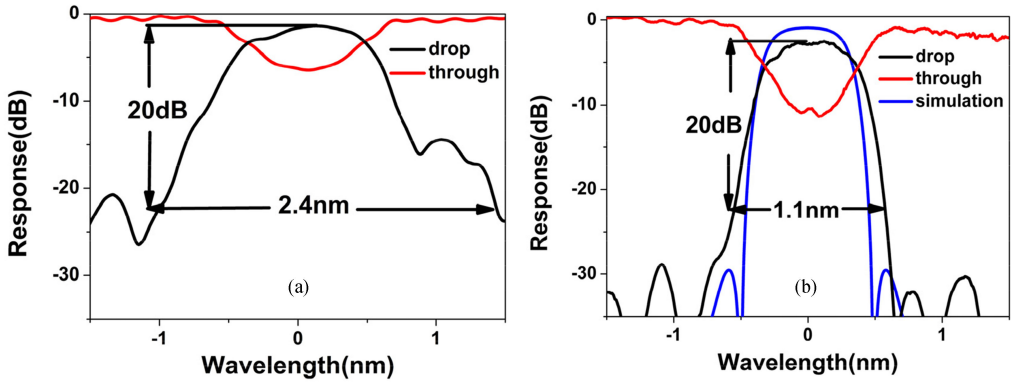

Fig. 3. Measured and simulated spectral responses of the gratings. (a) A standalone contra-DC. (b) A pair of contra-DCs connected in the way shown in Fig. 1(a).

plasma-enhanced chemical vapor deposition (PECVD), then 100-nm-thick Ti/W heaters are formed by the lift-off technique. Subsequently, a 300-nm-thick protective SiO_2 layer is deposited to cover the device. Finally, the SiO_2 layer above the pad is removed to enable the contact with the probe.

At first, we measure the waveguide propagation loss and the coupling loss of the fiber grating coupler, which are $\sim$2 dB/cm and $\sim$6 dB at 1550 nm, respectively. Transmission spectra of a standalone contra-DC and a contra-DC pair connected in the manner shown in Fig. 1(a) then are characterized with a tunable laser (Santec TSL-510) and an optical power monitor (HP 8153A). Results are displayed in Fig. 3, where the coupling loss of the two fiber grating couplers has been normalized. The simulation result utilizing the finite difference time domain (FDTD) method is also plotted in Fig. 3(b). The drop port of the single contra-DC in Fig. 3(a) exhibits a SLSR of 19 dB and an insertion loss of $\sim$1.3 dB at the central wavelength. Its 3 dB and the 20 dB bandwidths are 0.9 nm and 2.4 nm, respectively, which hardly meet the requirement of the 200 GHz DWDM system. In contrast, the drop port of the contra-DC pair in Fig. 3(b) exhibits substantially reduced 3 dB and 20 dB bandwidths of 0.4 nm and 1.1 nm, respectively. Furthermore, a desirable box-like filtering response is obtained. The measured SLSR is enhanced to 26 dB. The penalty is that the insertion loss at the drop port rises to 2.6 dB. It is also observed that the extinction ratios of the through port spectra in both Figs. 3(a) and 3(b) are relatively low. As already analyzed in Section 2, if a better quality control of the SOI material and the processing is available, we can reduce the insertion loss of the drop port and improve the extinction ratio of the through port by increasing the grating length.

By cascading four pairs of grating assisted contra-DCs in series, we build a four channel tunable DWDM demultiplexer in another batch. The idea is to demonstrate a reconfigurable demultiplexer, so all four contra-DC pairs are identical. The channel selection is implemented by tuning the heating power. However, if the reconfigurability is not required, the four contra-DC pairs can be designed to have different central wavelengths that match the wavelength grid of the DWDM system. Measured spectral responses of all four drop ports as well as the through port are displayed in Fig. 4 with the coupling loss of fiber grating couplers being normalized. The central wavelengths of the four channels are separated with a uniform spacing of $\sim$1.6 nm by tuning heating powers. Thanks to the steep filtering characteristics and the strong sidelobe suppression, isolations between all adjacent channels are better than 20 dB. The insertion loss of the through port at off-resonance wavelengths is 0.6 dB, whereas those of the four drop ports at their respective central wavelengths are $<$3 dB. More information is given in Table 1. Compared with Fig. 3(b), spectra of drop and through ports in Fig. 4 present much stronger intra band ripples. It has been analyzed in [22] that these intra band ripples are mainly caused by the waveguide sidewall roughness induced phase noise. Therefore, we attribute intra band nonuniformities in Fig. 4 to the poor fabrication quality of this batch.

Without the FSR limitation, central wavelengths of the four-channel demultiplexer can be tuned through the whole C band in principle. In Fig. 5, thermal tunabilities of all four channels are charac-

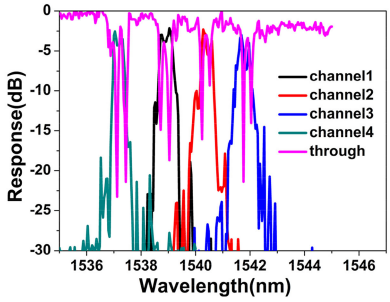

Fig. 4. Measured spectral responses of the four-channel DWDM demultiplexer.

TABLE 1
Measurement Results of Each Channel of the Four-Channel DWDM Multiplexer

	Loss(dB)	Center wavelength(nm)	20dB Bandwidth(nm)	Ripple level(dB)	Crosstalk(dB)
Channel1	-2.3	1537.1	0.78	1.5	<-20
Channel2	-2.6	1538.7	0.90	1.3	
Channel3	-2.7	1540.3	0.95	2.1	
Channel4	-3	1541.9	1.04	2.5	

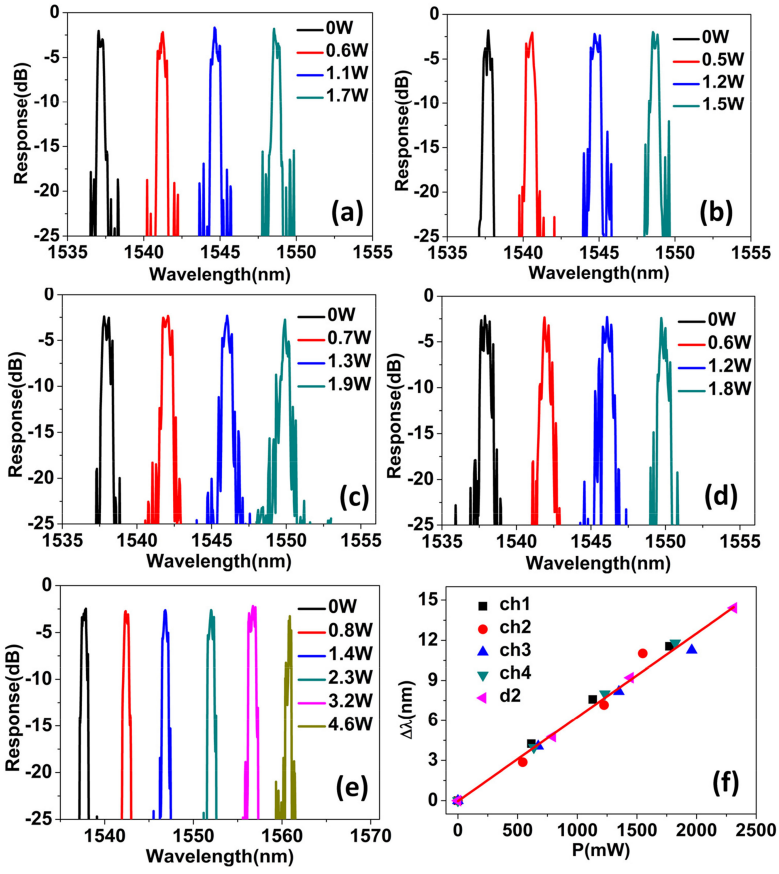

Fig. 5. (a)–(d) Measured spectral responses at four drop ports of the four-channel tunable DWDM demultiplexer upon different heater powers. The resistance of heaters is 800 Ω for this device. (e) Measured spectral responses of a single channel filter which consists of a grating assisted contra-DC pair. The resistance of heaters is 400 Ω. (f) Relationships between heater powers and wavelength shifts extracted from (a)–(e).

terized. As a result of the fabrication imperfection, the two contra-DCs of each channel have slightly different center wavelengths. In order to eliminate the disalignment of their center wavelengths, the thermal tuning powers on the two contra-DCs are slightly different as well. Values marked inside Fig. 5 denote the combined power of the two heaters. Resistances of all heaters are measured to be ∼800 Ω. As center wavelengths shift, insertion losses of all four channels remain at ∼3 dB. However, deteriorations of filtering curves are manifested by reduced SLSRs. The reason is that the thermal fields are not exactly uniform along 0.9-mm-long waveguide gratings. As the heater power increases, the longitudinal fluctuation of thermal field adds a phase noise to the grating apodization profile, and hence distorts spectral responses in Fig. 5. Wavelength tuning ranges in Figs. 5(a)–5(d) are ∼12 nm, which are constrained by the 32 V maximum output of our voltage source. The average thermal tuning efficiency of four channels is 0.006 nm/mW as shown in Fig. 5(f), where shifts of center wavelengths are plotted as a function of the heater power. In Fig. 5(e), we measure another contra-DC pair whose heater width is doubled from 4 μm to 8 μm. Thanks to the halved resistance of 400 Ω, a tuning range of 25 nm is achieved with the same voltage source. It is noteworthy that filtering curves are subjected to less deterioration in Fig. 5(e) than those in Figs. 5(a)–5(d) while devices are heated. It implies that the longitudinal uniformity of the thermal field can be improved by widening the electrode.

4. Conclusion

In conclusion, we demonstrate a four-channel tunable demultiplexer based on silicon grating-assisted contra-DCs. The device possesses merits of narrow bandwidth, box-like filtering response, and FSR free operation, which are strongly desired by DWDM systems. Despite these advantages, there are two issues need to be addressed in future. At first, compared with ring based demultiplexers, power consumptions for thermal tuning are high as a result of large volumes of silicon WBGs. Secondly, the filtering responses present discernible deteriorations as central wavelengths are shifted by heaters. In view of these issues, following works are suggested for future: globally optimizing the layout so as to improve the uniformity of the thermal field along the grating, utilizing techniques such as the BOX layer undercutting to enhance the heating efficiency [23], reducing the insertion loss by increasing the grating length. In addition, if the wavelength reconfigurability is not necessary, the four-channels can be designed with different central wavelengths by adjusting their grating periods. By this way, the central wavelength of each channel only needs to be tuned slightly so as to compensate the disalignment caused by fabrication errors, the total power consumption therefore can be reduced substantially.

Acknowledgment

The authors would like to thank the training platform of information and microelectronic engineering in polytechnic institute of Zhejiang university.

References

[1] Y. Hung, K. H. Lin, C. Wu, C. Y. Wang, and Y. J. Chen, "Narrowband reflection from weakly coupled cladding-modulated bragg gratings," *IEEE J. Sel. Topics Quantum Electron.*, vol. 22, no. 6, Nov./Dec. 2016, Art. no. 4402507.
[2] Q. Huang, Q. Liu, and J. Xia, "Traveling wave-like fabry-perot resonator-based add-drop filters," *Opt. Lett.*, vol. 42, no. 24, pp. 5158–5161, 2017.
[3] K. Okamoto, "Wavelength-division-multiplexing devices in thin SOI: Advances and prospects," *IEEE J. Sel. Topics Quantum Electron.*, vol. 20, no. 4, pp. 248–257, Jul./Aug. 2014.
[4] W. Bogaerts *et al.*, "Silicon-oninsulator spectral filters fabricated with CMOS technology," *IEEE J. Sel. Topics Quantum Electron.*, vol. 16, no. 1, pp. 33–44, Jan./Feb. 2010.
[5] W. Bogaerts *et al.*, "Silicon microring resonators," *Laser Photon. Rev.*, vol. 6, no. 1, pp. 47–73, 2012.
[6] D. G. Rabus, *Integrated Ring Resonators: The Compendium*. Berlin, Germany: Springer, 2007.
[7] D. A. I. Marpaung, C. G. H. Roeloffzen, R. G. Heideman, A. Leinse, S. Sales, and J. Capmany, "Integrated microwave photonics," *Laser Photon. Rev.*, vol. 7, no. 1, pp. 1–33, 2013.
[8] H. Qiu *et al.*, "FSR-free add–drop filter based on silicon grating-assisted contradirectional couplers," *Opt. Lett.*, vol. 38, no. 1, pp. 1–3, 2013

[9] W. Shi *et al*., "Ultra-compact, flat-top demultiplexer using anti-reflection contra-directional couplers for CWDM networks on silicon," *Opt. Exp*., vol. 21, no. 6, pp. 6733–6738, 2013.
[10] H. Qiu *et al*., "Silicon band-rejection and band-pass filter based on asymmetric Bragg sidewall gratings in multimode waveguide," *Opt. Lett*., vol. 41, no. 11, pp. 2450–2453, 2016.
[11] H. Okayama, Y. Onawa, D. Shimura, H. Yaegashi, and H. Sasaki, "Polarization rotation Bragg grating using Si wire waveguide with non-vertical sidewall," *Opt. Exp*., vol. 22, no. 25, pp. 31371–31378, 2014.
[12] D. T. H. Tan *et al*., "Wide bandwidth, low loss 1 by 4 wavelength division multiplexer on silicon for optical interconnects," *Opt. Exp*., vol. 19, no. 3, pp. 2401–2409, 2011.
[13] J. St-Yves, S. LaRochelle, and W. Shi, "O-band silicon photonic Bragg-grating multiplexers using uv lithography," in *Proc. Opt. Fiber Commun. Conf*., 2016, paper Tu2F-7.
[14] D. T. H. Tan, A. Grieco, and Y. Fainman, "Towards 100 channel dense wavelength division multiplexing with 100 GHz spacing on silicon," *Opt. Exp*., vol. 22, no. 9, pp. 10408–10415, 2014.
[15] W. Shi, H. Yun, C. Lin, J. Flueckiger, N. A. F. Jaeger, and L. Chrostowski, "Coupler-apodized bragg-grating add-drop filter," *Opt. Lett*., vol. 38, no. 16, pp. 3068–3070, 2013.
[16] J. Jiang *et al*., "Silicon lateral-apodized adddrop filter for on-chip optical interconnection," *Appl. Opt*., vol. 56, no. 30, pp. 8425–8429, 2017.
[17] W. Shi *et al*., "Silicon photonic grating-assisted, contra-directional couplers," *Opt. Exp*., vol. 21, no. 3, pp. 3633–3650, 2012.
[18] J. St-Yves, H. Bahrami, P. Jean, S. LaRochelle, and W. Shi, "Widely bandwidth-tunable silicon filter with an unlimited free-spectral range," *Opt. Lett*. vol. 40, no. 23, pp. 5471–5474, 2015.
[19] M. T. Boroojerdi, M. Ménard, and A. G. Kirk, "Wavelength tunable integrated add-drop filter with 10.6 nm bandwidth adjustability," *Opt. Exp*., vol. 24, no. 19, pp. 22043–22050, 2016.
[20] R. Liu, Y. Wang, D. Yin, H. Ye, X. Yang, and Q. Han, "A high-efficiency grating coupler between single-mode fiber and silicon-on-insulator waveguide," *J. Semicond*., vol. 38, no. 5, pp. 78–81, 2017.
[21] A. D. Simard, Y. Painchaud, and S. LaRochelle, "Integrated Bragg gratings in spiral waveguides," *Opt. Exp*., vol. 21, no. 7, pp. 8953–8963, 2013.
[22] A. D. Simard, N. Ayotte, Y. Painchaud, S. Bedard, and S. LaRochelle, "Impact of sidewall roughness on integrated Bragg gratings," *J. Lightw. Technol*., vol. 29, no. 24, pp. 3693–3704, Dec. 2011.
[23] K. Chen, F. Duan, and Y. Yu, "High-performance thermos-optic tunable grating filters based on laterally supported suspend silicon ridge waveguide," *Opt. Exp*., vol. 26, no. 15, pp. 19479–19488, 2018.